Exp. Eye Res. (2002) **74**, 403–410
doi:10.1006/exer.2001.1134, available online at http://www.idealibrary.com on IDEAL®

Improved Leukocyte Tracking in Mouse Retinal and Choroidal Circulation

HEPING XU[a*], A. MANIVANNAN[b], KEITH A. GOATMAN[b], JANET LIVERSIDGE[a], PETER F. SHARP[b], JOHN V. FORRESTER[a] AND ISABEL J. CRANE[a]

[a]*Department of Ophthalmology, Aberdeen University Medical School, Aberdeen, Scotland, U.K. and* [b]*Department of Biomedical Physics and Bioengineering, Aberdeen University Medical School, Aberdeen, Scotland, U.K.*

(*Received Cleveland 4 June 2001 and accepted in revised form 22 October 2001*)

The purpose of this study is to develop a new method with which to visualize leukocyte dynamics in murine choroidal and retinal circulation. Both pigmented (B10.RIII) and non-pigmented (BALB/c) mice were used in this study. One hundred µl of 0·05 % sodium fluorescein was injected via the mice tail vein to outline the vessel, followed by 150 µl (10^7 cells) C-AM labelled leukocytes. Fundus images were obtained with a confocal scanning laser ophthalmoscope. The dynamic image sequences were recorded simultaneously on videotape (S-VHS) and digitally at 25 frames per sec. The digital images were later analysed with a custom-made personal computer-based image analysis system. Both the choroidal and retinal circulation can be visualized in non-pigmented mice in the first few seconds of fluorescein angiography. However, the view of the choroidal and the retinal capillary circulation is soon blurred due to the rapid fluorescein leakage in the choroid. In contrast, in pigmented mice, retinal circulation is clear against the dark background of the choroid, while choroidal circulation is masked behind the pigment epithelial layer and cannot be seen at all. C-AM labelled leukocytes were clearly seen in the retinal circulation of all experimental mice and in the choroidal circulation of non-pigmented mice for as long as 30 min. The number of labelled circulating cells decreased as time clasped. Cells moved rapidly in the retinal arteries, slowing down or even stopping for a few seconds in the capillary system, and then moved slightly faster again through the postcapillary venules and veins. In non-pigmented mice, significant number of cells were seen to have arrested in the choroidal circulation. There was no difference between B10.RIII mice and BALB/c mice in vessel diameters, leukocyte velocities and shear stresses. This method allows the visualization of leukocytes and provides data on their behavior as they move through the choroidal and retinal circulation of non-pigmented mice, and in the retinal circulation of pigmented mice. It provides a valuable new tool for the investigation of real time leukocyte dynamics in murine retinal and choroidal microcirculations both under physiological conditions and during the development of ocular disease.

Key words: scanning laser ophthalmoscopy; leukocyte; retina; choroid; circulation; image; mice.

1. Introduction

Leukocyte–endothelial cell interactions play an important role in the pathogenesis of various types of retinal vascular diseases, including diabetes (Schroder et al. 1991; Miyamoto et al., 1998), uveitis (Miyamoto et al., 1996; Parnaby-Price et al., 1998) and ischemic diseases (Hatchell, Wilson and Saloupis, 1994). Recently, several methods have been developed which use scanning laser ophthalmoscopy (SLO) to study leukocyte dynamics in vivo in the retinal circulation under physiological as well as pathologic conditions (Fillacier et al., 1995; Kimura et al., 1995; Nishiwaki et al., 1995; Yang et al., 1996). Previously a non-invasive in vivo leukocyte tracking method was reported using confocal SLO in rat (Hossain et al., 1998). Leukocyte velocities within the retinal and choroidal circulations were quantified simultaneously using only a single image (Hossain et al., 1998). None of the former methods have been developed for mice, mainly due to problems arising from the small size of the mouse eye. However, there are many advantages of using a murine model to study retinal vascular disease such as enhanced genetic definition, increased range of available reagents and cost reduction. The authors have, therefore, developed a method which allows the tracking of leukocytes in the retinal circulation of both non-pigmented and pigmented mice, and in the choroidal circulation of non-pigmented mice.

2. Materials and Methods

Animals

Female B10.RIII and BALB/c mice, 8–12 weeks old, weighing approximately 20 g bred in the Biological Services Unit, University of Aberdeen were used as both sources and recipients of lymphoid cells. All the

* Address correspondence to: Heping Xu, Department of Ophthalmology, Aberdeen University Medical School, Foresterhill, Aberdeen AB25 2ZD, Scotland, U.K. E-mail: h.xu@abdn.ac.uk

0014-4835/02/030403+08 $35.00/0

animals were managed in accordance with the ARVO Statement for the Use of Animals in Ophthalmic and Vision Research and under the United Kingdom Animal License Act (1986).

Cell Labeling with Calcein-AM

A single cell suspension was prepared from normal B10.RIII or BALB/c mouse spleen according to a previous description (Hossain et al., 1998). Cells were resuspended in 20 ml complete medium [RPMI 1640 supplemented with 10 % (v/v) heat-inactivated fetal calf serum, 1 % sodium pyruvate, 4 mM L-glutamine, 100 μ ml^{-1} streptomycin and 100 IU ml^{-1} penicillin, Gibco BRL, Paisley, U.K.]. 2×10^7 cells in 10 ml complete medium were incubated with 40 μg ml^{-1} calcein-AM (C-AM, Molecular Probes Europe BV, Leiden, The Netherlands) at 37°C for 30 min. Cells were then washed twice and adjusted to 1×10^7 cells in 150 μl medium and kept on ice until the SLO study (within 30 min).

In vivo Cell Tracking using SLO

Mice were anesthetized with an intramuscular injection of 0·4 ml kg^{-1} Hypnorm (Janssen-Cilag Ltd, Belgium, U.K.) and 1 ml kg^{-1} Diazepam (Phoenix Pharmaceuticals Ltd., Gloucester, U.K.) intraperitoneally, producing deep anesthesia for 45 min. Pupils were dilated with one drop of 0·5 % (w/v) Tropicamide (Chauvin Pharmacerticals Ltd., Essex, U.K.). A hard contact lens (clear polymethymethacrylate, PMMA; refractive index, 1·51; radius of curvature, 1·7 mm; diameter, 3·2 mm; Cantor & Nissel, Northamptonshire, U.K.) was placed on the mouse cornea to obtain a clear view of the fundus. In addition, a +25D lens was placed 1 cm in front of the mouse cornea to further focus the laser beam and correct for the refractive error of the mouse eye. This lens also increased the field of view. 100 μl of 0·05 % (v/v) sodium fluorescein (Sigma, Poole, U.K.) was injected via the tail vein to outline the vessels, followed by 1×10^7 C-AM-labelled cells in 150 μl complete medium. The physiological conditions of the animals were monitored in a parallel experiment. They were: heart beat rate, 325–500 beats per min, and body temperature between 34·7° and 36·4°C.

The mouse fundi were examined using a custom built SLO (Manivannan et al., 1993). In each animal three fundus areas adjacent to the optic disc were chosen. The animal was positioned so that a retinal artery and vein could be viewed in each area. A collimated argon laser (wavelength 488 nm, power 1 mW) with a diameter of 1 mm was used to excite fluorescence. A 515 nm barrier filter was used in the return path to enable detection of fluorescing cells without interference from the incident laser light. The images were collected digitally using a frame grabber (Meteor, Matrox, Swindon, U.K.) interfaced to a PC with an image matrix size of 768 × 526 pixels and 256 gray levels. Images were recorded simultaneously on videotape (S-VHS). At least 900 frames were recorded digitally at 25 frames per sec intermitted within the first 15 min following injection of the labelled cells, and were subsequently used for image analysis (vessel diameter and cell velocity). The videotape recording was used for circulating and sticking cells analysis.

Estimating the Pixel Size for the Mouse Fundus

To convert measured distances in pixels to micrometers, the pixel size was estimated by comparison of the SLO images and flatmounted confocal laser microscope images of the same retina. Six eyes from three mice were used. After acquiring the SLO images the mice were injected with 100 μl 2 % (w/v) Evans Blue (Sigma, Poole, U.K.) via the tail vein. The animals were then killed 10 min later by CO_2 inhalation. The eyes were removed and immediately immersed in 2 % (w/v) paraformaldehyde (Agar Scientific Ltd., Cambridge, U.K.) for 1 hr. Whole flat retinas were prepared in accordance with the method of Chan-Ling (1997). Retinal flatmounts were examined using a confocal scanning laser microscope fitted with krypton/argon lasers (Bio-Rad Microsciences MRC 1024, Hemel Hempstead, U.K.). A definable distance (for instance from one vessel branch to another) was measured in both confocal laser microscope images (μm, Fig. 1(B)) and SLO images (pixels, Fig. 1(A)). The size of a squire pixel was thus calculated to be 3 ± 0.24 μm.

Measuring Leukocyte Velocity

The SLO uses interlaced scanning (Manivannan et al., 1993), where each digitized frame consists of two fields; an odd field (containing odd-numbered horizontal scan lines) and an even field (containing even-numbered horizontal scan lines). Each field requires 20 msec to scan from top to bottom. For typical cell velocities present in the mouse eye this means that the cell position changes significantly between the odd and even fields, resulting in two, striped images of the same cell on a single video frame. The authors have described in a previous publication how this effect was exploited to measure cell velocity using only a single video frame (Hossaain et al., 1998). Measurement in the central arteries and veins using multiple frames is usually impossible because the high cell velocities mean that the cell leaves the field of view after only a single frame.

This method has been refined here: (1) to take into account the finite time required for the SLO to scan all the lines in the image and (2) to allow for non-linear cell trajectories. The scan time correction was necessary for cells which move vertically in the image plane (perpendicular to the scan lines); otherwise cells which are moving towards the top of the image (Fig. 2(A)). result in an overestimate of the time elapsed between

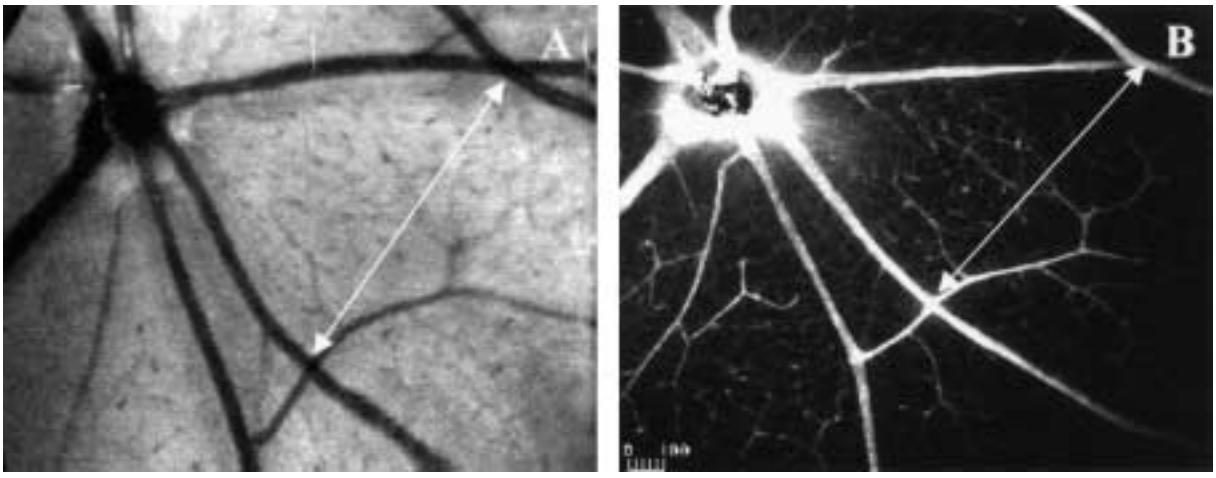

FIG. 1. Confocal microscope and SLO image of a mouse retina. A mouse fundus image was captured using SLO (A). Just after SLO, a retinal flatmount was prepared and observed by a Bio-Rad confocal laser microscope (B). The distance from one vessel branch to another was measured and shown to be in pixels (A) and μm (B). The size of a squire pixel was calculated accordingly to be 3 μm. Scale in (B): μm.

appearances, leading to an underestimation of the velocity (the opposite being true for cells moving towards the bottom of the image (Fig. 2(B))). Without any correction the error in the final velocity value ranges from 0 to ± 100 %. No correction is made for the horizontal scan time of 64 μsec which results in an error in the velocity between 0 and ± 0·3 %. The time t between sightings, taking into account vertical cell motion in the image plane, is given by

$$t = T_{\mathrm{f}}\left(1 + \frac{l_2 - l_1}{N_1}\right),$$

where T_{f} is the time per field (20 msec), l_1 is the scan line the object center of mass is on in the first field, and l_2 the equivalent scan line in the second field, and N_{l} is the number of scan lines in each field.

Parameters

During data acquisition, the authors differentiated between artery/arteriole and vein/venule by the direction of blood flow because fluorescent staining patterns did not distinguish artery/arteriole and vein/venule morphologically. Cell velocities in central retinal arteries and veins within 1 mm from the optic disc, pre-capillary arterioles (PCAs), post-capillary venules (PCVs), and capillaries were analysed. A PCA is defined as the vessel which comes from an arteriole and goes into a capillary, whereas several capillaries

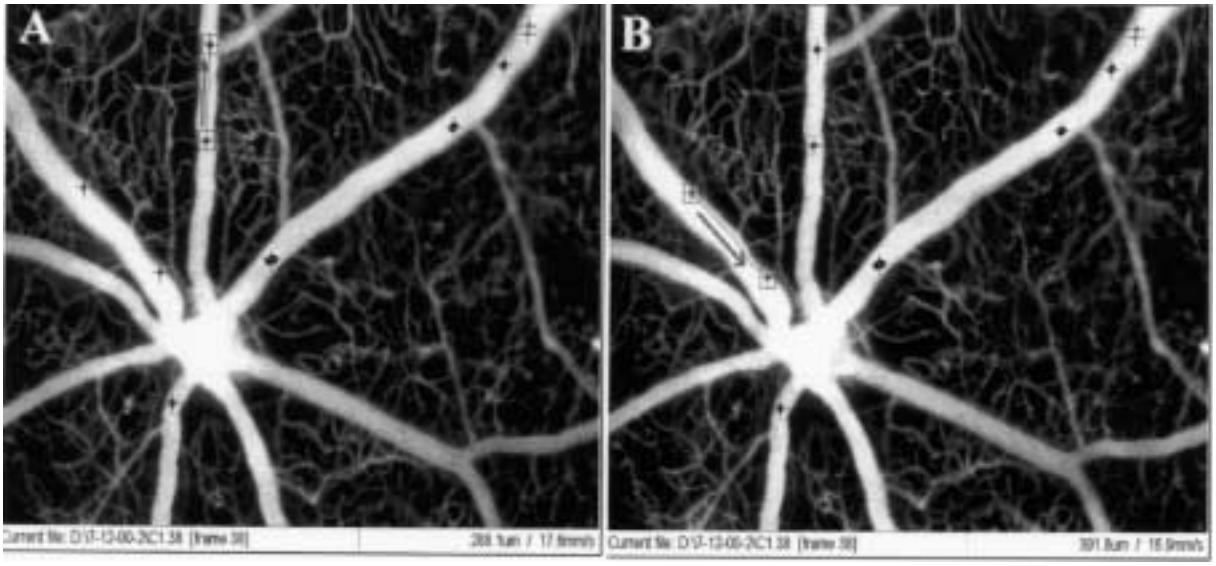

FIG. 2. Leukocytes velocities in SLO images measured by a refined computer program. Striped cells are labelled with either red (the odd field) or blue (the even field). Cell velocities are shown in the bottom right of each picture. (A) A cell moving upwards taking less time between appearances after adjustment for scanning time. (B) A cell moving downwards taking more scanning time between appearances. Thus even though the distance moved in (B) (391·8 μm) is further than that in (A) (288·1 μm), the velocity is lower.

come together to form a PCV which then drains into a venule. Measurements of the diameters of the central artery and vein were performed within 1 mm of the optic disc. The inner diameter of the vessel segment was assessed by three equally distributed measurements over the whole segment. The mean of these measurements was used for further calculations of shear stress.

Blood velocity (mm sec^{-1}) was determined by measuring the distance travelled by free-floating leukocytes in the vessel. Hemodynamic properties were calculated according to House and Lipowsky (1987). Mean red blood cell (RBC) velocity was calculated as $V_{mean} = V_{WBC}/1{\cdot}6$. Wall shear rate ($\gamma$) was calculated based on the Newtonian definition, $\gamma = 8(V_{mean}/\text{diameter})$, and wall shear stress was $\gamma \times$ blood viscosity (House and Lipowsky, 1987), where blood viscosity was assumed to be 0·025 poise (Lipowsky, Usami and Chien, 1980). Sticking (adherent) leukocytes were defined as such when firmly adherent to the vessel for 20 sec or longer.

Statistical Analysis

All data are presented as the mean $\pm$ S.E.(M.). For the statistical analysis of these results, unpaired Student's *t*-test was used.

3. Results

Fluorescein Angiography of the Mouse Fundus

Using the confocal SLO, a 43 × 32 degree field of mouse fundal view was captured. Both the retinal and choroidal vessels were visualized in non-pigmented mice (BALB/c) during the first few seconds of fluorescein angiography. However, as the fluorescein leaked out of the choroidal vessels, the fundus background became brighter and thus the contour of choroidal vessels was no longer definable. Nevertheless, the retinal vessel system was still clearly visible for at least 30 min. In contrast, in pigmented mice (B10.RIII), the retinal microcirculation is clearly visible against the dark background of the choroid, while the choroidal circulation is masked behind the pigment epithelial layer and cannot be visualized at all. Fig. 3(A)–(C) shows the different phases of fluorescein angiography in a B10.RIII mouse. The initial retinal flush (arterial phase) was observed 1·68 $\pm$ 0·19 sec after injection of sodium fluorescein via the tail vein (Fig. 3(A)). After a further 0·67 $\pm$ 0·04 sec, the early arterio-venous phase can be distinguished with the whole retinal capillary network discernible. During the late stage of the arterio-venous phase, the retinal veins are beginning to fill with fluorescein (Fig. 3(B)). The early venous phase is 0·73 $\pm$ 0·01 sec later and at this stage almost all of the retinal veins are fully filled, and the entire retinal capillary architecture can be distinguished (Fig. 3(C)).

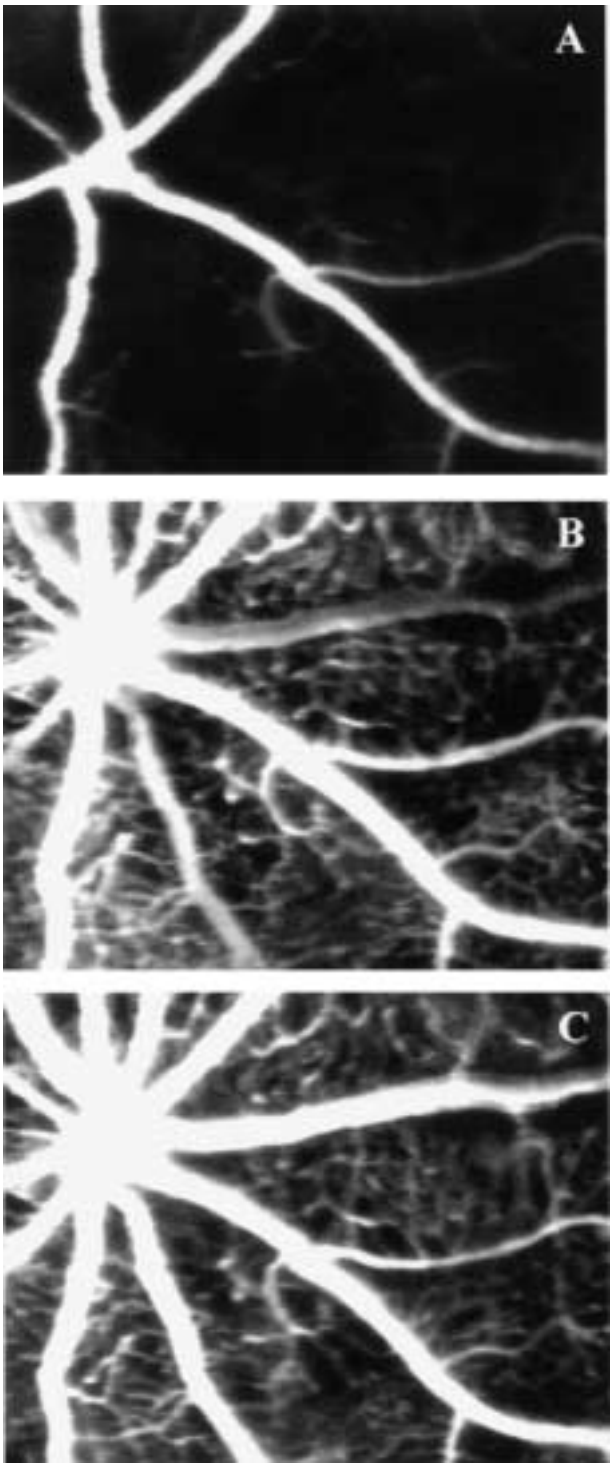

FIG. 3. Fluorescein angiograms of a normal B10.RIII fundus. (A) Arterial phase: the retinal arteries are fluorescent, the retinal veins and capillaries cannot be seen. (B) Arterio-venous phase: the capillaries are already filling with dye. The flow of dye in the retinal veins is laminar. (C) Venous phase: the retinal veins are fully filled and the entire retinal capillary architecture can be distinguished.

Using a confocal aperture of 100 μm the different layers of the fundus can be distinguished. Fig. 4(A) shows the superficial layer of the retina. The major

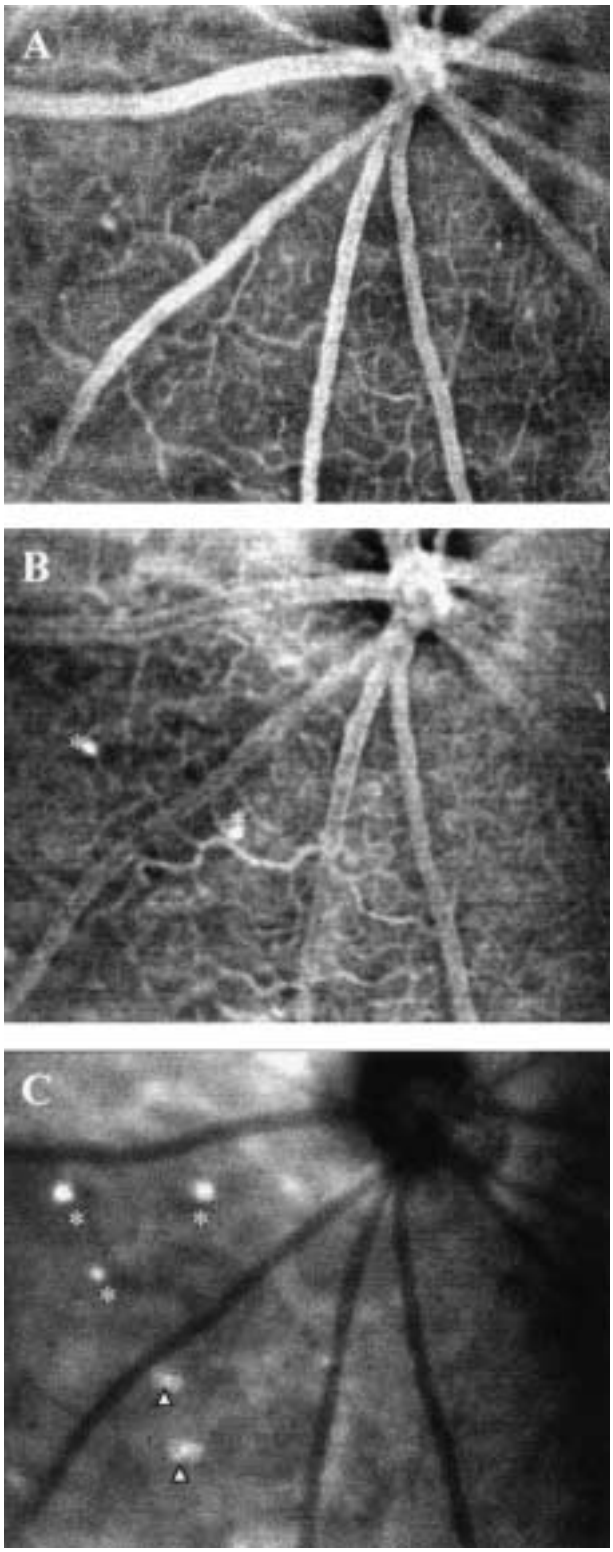

FIG. 4. Confocal SLO images of a BALB/c mouse fundus. (A) Superficial layer of the retina. (B) Deeper retinal layer: the outer retinal vascular plexus can be distinguished. Stars, sticking cells. (C) Choroidal layer: the retinal vasculature is less distinct (appears dark); cells sticking (star) moving (arrow head) in the choroidal circulation can be seen.

retinal vessels can be observed as well as the superficial retinal capillary plexus. Fig. 4(B) shows the retinal layers where the deeper retinal capillary plexus can now be distinguished. As the confocal plane moves deeper, the retinal vasculature is less distinct and forms a shadow (i.e. the retinal vessels appear dark) over the choroidal circulation (in BALB/c mice) which appears as a diffuse fluorescent layer as shown in Fig. 4(C).

Leukocyte Tracking in Retinal and Choroidal Circulation

In all experiments, circulating fluorescent cells were seen in the retina and in the non-pigmented choroid. All cells appeared brightly fluorescent against the fainter fluorescence of the sodium fluorescein. In the retinal circulation, labelled cells emerged at the optic disc and were distributed between the different arteries. They were clearly visualized leaving the main arteries prior to entering the capillary network, and returning to a vein. Some cells within the capillary system were seen to stop for a few seconds before joining a main vein. Occasionally, without slowing down, some cells stopped suddenly for a few seconds near a vein branch, then quickly moved away. Very few cells (two to five cells per eye) were found sticking for more than 1 min.

In non-pigmented mice, although the choroidal vessels became blurred rapidly due to the diffuse fluorescein, labelled fluorescent leukocytes could be observed within for up to 30 min, and could be seen to move randomly, despite being less distinct than those in the retinal circulation. It was difficult to assess in which choroidal vascular layer cell movement was taking place. Many more cells were found to be adherent in the choroids than in the retina ($P < 0{\cdot}001$, Figs 5(B), 4(B) and 4(C)).

The number of circulating fluorescent cells was found to decline gradually as time elapsed (Fig. 5(A)), although after 30 min, many fluorescent leukocytes could still be detected in retinal vessels in both pigmented and non-pigmented mice. Fewer circulating fluorescent cells were found in the retinal circulation of non-pigmented mice than pigmented mice ($P < 0{\cdot}05$, Fig. 5(A)).

Vessel Diameters and Leukocyte Velocities

The average retinal vessel diameters, cell velocities and the shear stress of different vessels are shown in Table I. The results show that the diameter of the central retinal veins is larger than that of the central retinal arteries. Cells moved faster in the retinal arteries and slowed down before entering the capillaries. Within the capillaries the cells moved very slowly but the velocities were increased throughout the PCVs and veins. There was no significant difference in the vessel diameter, leukocyte velocities and shear stresses between B10.RIII mice and BALB/c mice.

4. Discussion

The authors report herein a non-invasive, real-time, in vivo leukocyte tracking method which

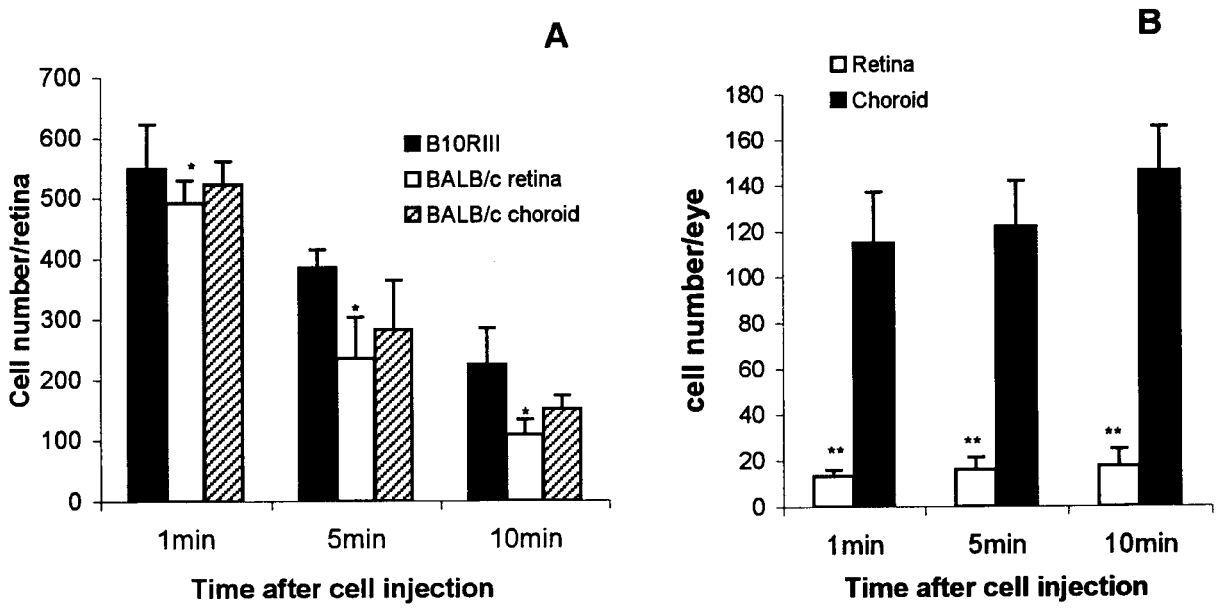

FIG. 5. Fluorescent circulating and adherent cells in retinal and choroidal circulations. (A) Circulating cell: labelled circulating cells declined gradually. More circulating cells were observed in the retina of B10.RIII mice ($n = 5$) than BALB/c mice ($n = 3$) at each time point (*$P < 0{\cdot}05$). (B) Adherent cells in BALB/c mice: more adherent cells were found in the choroid than in the retina (**$P < 0{\cdot}001$, $n = 3$).

TABLE I

Vessel diameters, leukocyte velocities and shear stresses in B10.RIII and BALB/c mice [mean ± S.E.(M.)]

	B10.RIII mice ($n = 5$)	BALB/c mice ($n = 3$)
Vessel diameter (μm)		
Arteries*	57·30 ± 1·38	58·63 ± 1·28
Veins*	74·06 ± 1·95	67·92 ± 2·42
Cell velocities (mm sec^{-1})		
Arteries*	20·63 ± 0·70	22·47 ± 1·21
Veins*	18·03 ± 1·32	19·90 ± 1·32
PCAs	10·77 ± 0·62	9·37 ± 1·37
PCVs	7·13 ± 0·52	6·26 ± 0·90
Capillaries	2·29 ± 0·15	2·42 ± 0·12
Choroid		3·76 ± 0·39
Shear stress (dyn cm^{-2})		
Arteries*	46·14 ± 1·86	48·76 ± 2·67
Veins*	31·99 ± 0·70	37·95 ± 1·78

*Central retinal arteries and veins.

enables the behavior of individual leukocytes circulating through the murine retina and choroid to be visualized in terms of velocity and contact with the endothelium. The advantages of this method are: firstly, the leukocytes are labelled with C-AM which is non-toxic and has no effect on cell adhesion (Abbitt, Rainger and Nash, 2000); secondly, only one image frame containing a moving cell is required to measure the velocity of the leukocyte; and finally, the additional lens allows the authors to image a larger area of the retina (43 × 32 degree field of view) than that achieved in their earlier work (Hossain et al., 1998), enabling the measurement of leukocyte velocities in the central arteries and veins.

Due to the small size of the mouse eye, it is difficult to visualize the vessels of the mouse retina using a normal SLO. In the present study a higher resolution image and higher magnification SLO were used. In addition, there are two other technical problems which restrict imaging of the mouse retina. Firstly, the mouse eye comprises a relatively large lens and short axial length. During SLO, the pupil is dilated and the large pupil leads to a reduction of the image quality as a result of spherical aberration. To avoid this

distortion, an extra lens (+25D) is placed 1 cm in front of the mouse eye to further focus the laser beam. This ensures that most of the laser beam passes through the centre of the mouse lens, reducing the spherical aberration. The second problem is the effect of corneal drying. The corneal–air interface is the principle refracting surface in the eye and its integrity is preserved by the tear film which is maintained by various lacrimal secretions and a regular blink reflex. An intact corneal tear film is paramount for clear fundal imaging. During general anesthesia both the blink reflex and aqueous tear production are reduced, disrupting the tear film, leading to poor quality fundal images. The use of a contact lens effectively solves this problem. Contact lenses also keep the mouse eye open during SLO examination, thus avoiding the use of a speculum.

The majority of other SLO studies (Fillacier et al., 1995; Nishiwaki et al., 1995; Kinukawa et al., 1999) have measured the velocity by superimposing consecutive frames. The time interval between cell positions is assumed to be the time taken to scan a frame. However, as it was stated earlier, the time is dependent on the direction of motion because of the finite time taken to scan a frame. This is particularly significant in the central arteries and veins where the velocities are higher and consequently also the errors. The current study also permits the measurement of distances through tortuous vessels, allowing measurements to be made in both large and small vessels.

This study gave similar results for vessel diameters, leukocyte velocities, as well as shear stresses in both B10.RIII mice and BALB/c mice. The flow velocities of the leukocytes moving in the retinal artery in the present study are similar to the leukocyte velocities in the human retinal artery (7–21 mm sec^{-1}) (Paques et al., 2000). However, the leukocyte velocities in the mouse retinal vein and capillary were higher than those of humans (4·7–11 mm sec^{-1} in major veins, $1{\cdot}43 \pm 1{\cdot}3$ mm sec^{-1} in macular capillaries and $1{\cdot}82 \pm 1{\cdot}4$ mm sec^{-1} in the peripapillary capillaries) (Paques et al., 2000), and rats ($1{\cdot}58 \pm 0{\cdot}23$ mm sec^{-1} in capillary) (Kinukawa et al., 1999). Furthermore the diameters of the retinal vessels in the present study were found to be larger than those reported for rat retinal vessels ($32{\cdot}6 \pm 3{\cdot}7$ μm for arteries and $49{\cdot}8 \pm 4{\cdot}5$ μm for veins) (Hamada et al., 1997). The variations may be due to the difference in species, measurement sites, or the different measurement methodology.

Transient plugging of vessels by leukocytes has been observed in the capillaries under physiological and pathologic conditions in rats and rabbits (Nishiwaki et al., 1995; Yang et al., 1996; Hossain et al., 1998). The majority of leukocytes remained stationary for less than 1 sec. In this study, a similar phenomena was found in mouse retinal and choroidal circulation. Although only few of them stopped for as long as 20 sec (about six times the recirculation time in the mouse) or more, many more adherent leukocytes were found in choroidal circulation than in retinal circulation. The difference observed may reflect anatomic differences between the fenestrated endothelium of the choroids and the microvascular endothelium of the inner blood–retina barrier or different levels of adhesion molecule expression by those two cell types in vivo.

Fewer circulating fluorescent cells were found in the retinal circulation of non-pigmented mice than pigmented mice. This is probably because the bright choroidal fluorescent background in the non-pigmented mice masked some of the fluorescent cells in the retinal circulation. The number of circulating fluorescent cells was found to decline gradually. However, the number of adherent cells in both the retina and the choroid did not increase significantly as time elapsed. Previous studies in the rat have shown that the majority of injected spleen leukocytes arrest in the lung, liver and spleen (Hossain, unpublished res.).

To the knowledge of the authors, this is the first study to visualize and measure leukocyte dynamics in the murine retinal and choroidal microcirculations. It provides detailed information on leukocyte behavior in the retinal and choroidal microcirculation under real physiological conditions and under flow and shear stress. The identification of factors important in the use of this type of technique is of increasing value as tracking of leukocytes is used clinically as a diagnostic tool (Paques et al., 2000). This non-invasive method will also be of value for the study of retinal hemodynamics in murine models of ocular disease particularly in EAU, diabetic retinopathy and retinal ischemia and in the evaluation of potential therapies involving leukocyte/endothelial interaction.

Acknowledgements

The authors thank Mr Hattam Atta and Ms Karon Robinson of the Eye Clinic, Aberdeen Royal Infirmary, for their help with the design of the mouse contact lens and Dr Yong-Hao Zhang, Engineering Department, Aberdeen University, for mathematical advice. They also thank Dr Thomas Engelhardt, Department of Anaesthesia and Intensive, Institute Medical Sciences, Aberdeen University, for the help with monitoring mouse general condition and the staff at the University of Aberdeen, Biological Unit, in particular, Ms Valerie Taylor for technical assistance. This work was supported by The Wellcome Trust, grant No. 057311.

References

Abbitt, K. B., Rainger, G. E. and Nash, G. B. (2000). Effects of fluorescent dyes on selectin and integrin-mediated stages of adhesion and migration of flowing leukocytes. *J. Immunol. Methods* **239**, 109–19.

Chan-Ling, T. (1997). Glial, vascular, and neuronal cytogenesis in whole-mounted cat retina. *Microsc. Res. Tech.* **36**, 1–16.

Fillacier, K., Peyman, G. A., Luo, Q. and Khoobehi, B. (1995). Study of lymphocyte dynamics in the ocular

circulation: technique of labeling cells. *Curr. Eye Res.* **14**, 579–84.

Hamada, M., Ogura, Y., Miyamoto, K., Nishiwaki, H., Hiroshiba, N. and Honda, Y. (1997). Retinal leukocyte behavior in experimental autoimmune uveoretinitis of rats. *Exp. Eye Res.* **65**, 445–50.

Hatchell, D. L., Wilson, C. A. and Saloupis, P. (1994). Neutrophils plug capillaries in acute experimental retinal ischemia. *Microvasc. Res.* **47**, 344–54.

Hossain, P., Liversidge, J., Cree, M. J., Manivannan, A., Vieira, P., Sharp, P. F., Brown, G. C. and Forrester, J. V. (1998). In vivo cell tracking by scanning laser ophthalmoscopy: quantification of leukocyte kinetics. *Invest. Ophthalmol. Vis. Sci.* **39**, 1879–87.

House, S. D. and Lipowsky, H. H. (1987). Leukocyte-endothelium adhesion: microhemodynamics in mesentery of the cat. *Microvasc. Res.* **34**, 363–79.

Kimura, H., Kiryu, J., Nishiwaki, H. and Ogura, Y. (1995). A new fluorescent imaging procedure in vivo for evaluation of the retinal microcirculation in rats. *Curr. Eye Res.* **14**, 223–8.

Kinukawa, Y., Shimura, M. and Tamai, M. (1999). Quantifying leukocyte dynamics and plugging in retinal microcirculation of streptozotosin-induced diabetic rats. *Curr. Eye Res.* **18**, 49–55.

Lipowsky, H. H., Usami, S. and Chien, S. (1980). In vivo measurements of apparent viscosity and microvessel hematocrit in the mesentery of the cat. *Microvasc. Res.* **19**, 297–319.

Manivannan, A., Sharp, P. F., Phillips, R. P. and Forrester, J. V. (1993). Digital fundus imaging using a scanning laser ophthalmoscope. *Physiol. Meas.* **14**, 43–56.

Miyamoto, K., Hiroshiba, N., Tsujikawa, A. and Ogura, Y. (1998). In vivo demonstration of increased leukocyte entrapment in retinal microcirculation of diabetic rats. *Invest. Ophthalmol. Vis. Sci.* **39**, 2190–4.

Miyamoto, K., Ogura, Y., Hamada, M., Nishiwaki, H., Hiroshiba, N. and Honda, Y. (1996). In vivo quantification of leukocyte behavior in the retina during endotoxin-induced uveitis. *Invest. Ophthalmol. Vis. Sci.* **37**, 2708–15.

Nishiwaki, H., Ogura, Y., Kimura, H., Kiryu, J. and Honda, Y. (1995). Quantitative evaluation of leukocyte dynamics in retinal microcirculation. *Invest. Ophthalmol. Vis. Sci.* **36**, 123–30.

Paques, M., Boval, B., Richard, S., Tadayoni, R., Massin, P., Mundler, O., Gaudric, A. and Vicaut, E. (2000). Evaluation of fluorescein-labeled autologous leukocytes for examination of retinal circulation in humans. *Curr. Eye Res.* **21**, 560–5.

Parnaby-Price, A., Stanford, M. R., Biggerstaff, J., Howe, L., Whiston, R. A., Marshall, J. and Wallace, G. R. (1998). Leukocyte trafficking in experimental autoimmune uveitis in vivo. *J. Leukocyte Biol.* **64**, 434–40.

Schroder, S., Palinski, W. and Schmid-Schonbein, G. W. (1991). Activated monocytes and granulocytes, capillary nonperfusion, and neovascularization in diabetic retinopathy. *Am. J. Pathol.* **139**, 81–100.

Yang, Y., Moon, S., Lee, S. and Kim, J. (1996). Measurement of retinal blood flow with fluorescein leucocyte angiography using a scanning laser ophthalmoscope in rabbits. *Br. J. Ophthalmol.* **80**, 475–9.